LARGE-SCALE AND SOLAR-CYCLE VARIATIONS OF THE SOLAR WIND

MARCIA NEUGEBAUER

Jet Propulsion Laboratory, California Institute of Technology, Pasadena, Calif. 91103, U.S.A.

Abstract. This paper summarizes space probe observations relevant to the determination of the large-scale, three-dimensional structure of the solar wind and its solar cycle variations. Observations between 0.6 and 5 AU reveal very little change in the average solar-wind velocity, but a pronounced decrease in the spread of velocities about the average. The velocity changes may be accompanied by a transfer of energy from the electrons to the protons. The mass flux falls off approximately as the inverse square of distance as expected for spherically symmetric flow. Measurements of the interplanetary magnetic field show that the spiral angle is well defined over this entire range of distances, but there is some evidence that the spiral may wind up more slowly with distance from the Sun than predicted by Parker's model. The variances or noise in the field and plasma have also been measured as a function of radial distance.

During the rising portion of the solar-activity cycle, the solar-wind velocity showed a pronounced positive correlation with solar latitude over the range $\pm 7°$. Several other plasma parameters which have been found generally to correlate (or anticorrelate) with velocity also showed a latitude variation; these parameters include the density, percent helium, and azimuthal flow direction. The average polarity and the north-south component of the magnetic field depend on the solar hemisphere in which the measurements are made.

Dependence on the phase of the solar-activity cycle can be found in the data on the number of high speed streams, the proton density, the percent helium, and the magnetic-field strength and polarity.

1. Introduction

There are many reasons for the interest in the large-scale and long-term variations of the solar wind. Some information about the sources of the solar wind can be derived from its dependence on latitude and solar activity. The solar wind is probably responsible for slowing down the rate of rotation of the Sun, but the Sun's average loss of angular momentum cannot be calculated without knowledge of the solar wind at all latitudes and at all phases of the solar-activity cycle. There are many interesting plasma-physics problems associated with the radial distribution of energy between the flow motion and stream structure, thermal motions of ions and electrons, the magnetic field, and waves and turbulence. It is now thought that, except following some solar flares, the solar wind comes from regions of open magnetic-field configuration and thus has little association with centers of solar activity. However, since both the cosmic-ray intensity and geomagnetic activity show pronounced solar-cycle variations, there must be a strong solar-cycle dependence of some of the properties of the solar wind. The modulation of cosmic-ray intensity is related to the large-scale, three-dimensional structure of the solar wind as well as to its time variations.

This is an appropriate time to attempt a review of the observations of large-scale and solar-cycle variations because of the recent success of Pioneer 10 in acquiring particle and field data out to 5 AU and because the solar wind has finally been observed in situ for longer than one 11-yr solar cycle. Unfortunately, there have been no high

Space Science Reviews **17** (1975) 221–254.

latitude observations, but the latitude modulations of the solar wind observed within 7° of the solar equator turn out to be surprisingly strong.

2. Radial Gradients

2.1. Solar-wind velocity

Radial gradients of the properties of the solar wind have been obtained in two ways – by time-series measurements on a spacecraft moving toward or away from the Sun and by simultaneous measurements by two or more spacecraft located at different positions along a solar radius vector. The first method has necessarily been used more extensively and yields fairly satisfactory results for parameters with steep radial gradients if large changes in distance from the Sun can be obtained. However, for those parameters which vary slowly with distance from the Sun, such as the solar-wind velocity, the time variations are often much larger than the gradient effects and the results are ambiguous. Thus no radial gradient can be discerned in the solar-rotation averages of the solar-wind velocity observed by either Mariner 2 (Neugebauer and Snyder, 1966) or Mariner 5 (Lazarus and Goldstein, 1971).

An example of the second approach is shown in Figure 1, taken from a paper by Lazarus *et al.* (1970). At the time of these observations, Mariner 5 and Explorer 34 were nearly on the same solar radius vector with Mariner 16×10^6 km closer to the Sun. The data plotted are hourly averages with the Mariner 5 observations of density corrected for the expected inverse-square dependence on distance from the Sun. The two sets of data show a high degree of correlation, but the short-term fluctuations and the changes in the velocity, density, and temperature profiles of the high-speed stream as it propagates from the Sun are too large to determine reliable average radial gradients of velocity or temperature. Similar studies by Intriligator and Neugebauer (1974), Dryer *et al.* (1974), and Mihalov *et al.* (1973) also yield more information about the propagation and evolution of stream structures than about the average radial variation of the speed of expansion of the solar wind.

Thus, the best information about radial velocity gradients comes from longer-term averages of the solar wind obtained by widely separated, intercalibrated spacecraft. Intriligator and Neugebauer (1974) compare the velocity observed near the Earth by OGO 5 with that observed by Pioneer 9 as it moved inward toward the Sun. The solar longitudes and latitudes of OGO and Pioneer differed by less than 12° and 0.1°, respectively, for the entire data set considered. Three-hour averages of velocity at OGO and Pioneer are paired according to the expected corotation delay time based on the velocity observed at Pioneer. Figure 2 shows the dependence of $(V_{\mathrm{OGO}} - V_{\mathrm{Pioneer}})/V_{\mathrm{OGO}}$ on the distance of Pioneer from the Sun; a negative value of $V_{\mathrm{OGO}} - V_{\mathrm{Pioneer}}$ corresponds to a deceleration of the solar wind as it moves outward. The outer error bars in Figure 2 are the standard deviations of the calculated average values and the inner bars are the expected standard *errors*. From Figure 2, one can estimate that any radial gradient between 1 and 0.81 AU is probably smaller than $\pm 10\%$ per AU. Averages over 0.2 AU intervals of the solar-wind velocity calculated

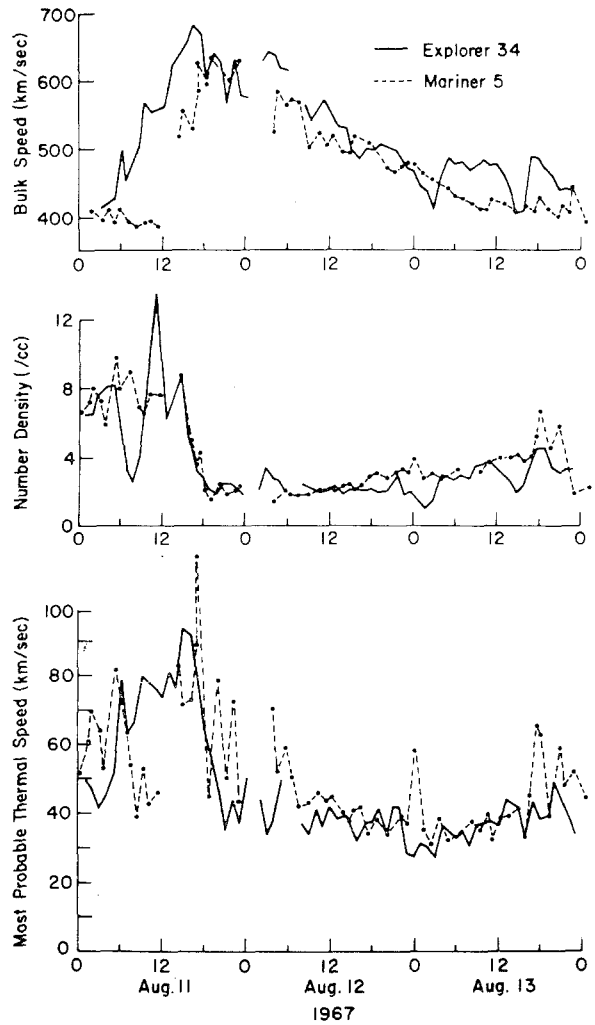

Fig. 1. Hourly averages of bulk speed, number density, and most probable thermal speed observed at Explorer 34 and Mariner 5 (Lazarus *et al.*, 1970).

from interplanetary scintillation measurements between 0.3 and 1.3 AU in 1973 are also consistent with no radial gradient (Coles *et al.*, 1974).

Pioneer 10 is now obtaining information about the properties of the solar wind over a much greater range of radial distances than previously possible. Some average velocities at Pioneer 10 compared to similar averages at other spacecraft at nearly the same longitude are given in Table I. The average decelerations are small and not inconsistent with radial expansion at constant velocity. The distribution of velocities, however, shows very significant changes with radial distance. The high velocity stream structure is less pronounced far from the Sun. A histogram of Pioneer-10 velocity measurements made between 4.1 and 4.7 AU is much narrower than the corresponding

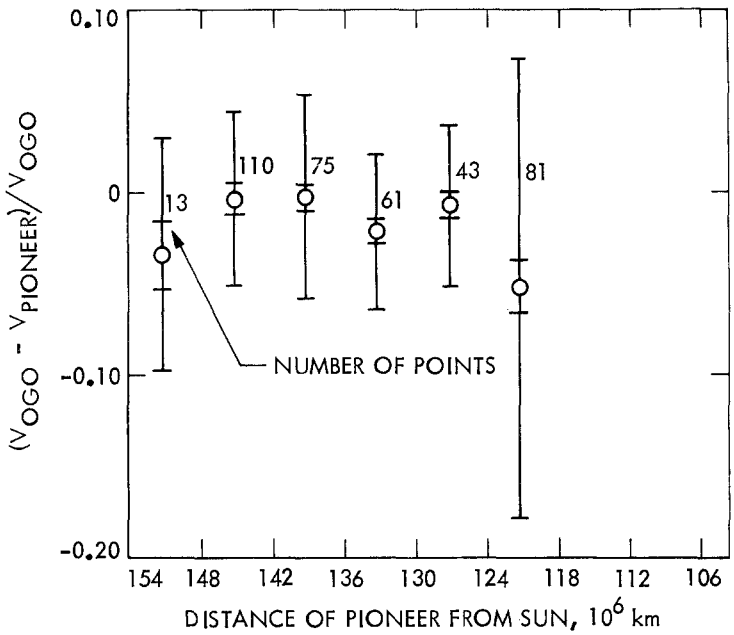

Fig. 2. Relative difference in three-hour averages of velocity at OGO-5 and Pioneer 9 as a function of the distance of Pioneer 9 from the Sun. The outer error flags represent the standard deviations of the measurements and the inner error flags are the standard errors expected for ideal, statistically independent data.

TABLE I

Simultaneous velocity observations by radially aligned pioneer spacecraft

Spacecraft	R(AU)	V(km s^{-1})
P11/P10	1.5/4.0	470/465
P8/P10	1.1/2.9	406/388
P11/P10	(1.0–2.1)/(4.1–4.7)	510/490

histogram of velocities at Pioneer 11 between 1.0 and 2.1 AU; after exclusion of the highest and lowest 5% of the velocity measurements, the range of 135 daily velocity samples was 265 km s^{-1} at Pioneer 10 compared to 380 km s^{-1} at Pioneer 11. The spread of velocity observed during each day was also less at Pioneer 10 than at Pioneer 11. (These Pioneer data are taken from Collard *et al.* (1973) and a presentation by J. H. Wolfe at the Third Solar Wind Conference, March, 1974.) Some of these effects can be seen in Figure 3, which shows the preliminary hourly averages of velocities observed during the August, 1972 disturbances by Pioneer 10 at 2.2 AU and Pioneer 9 at 0.77 AU. Note that different velocity scales are used for the two sets of data.

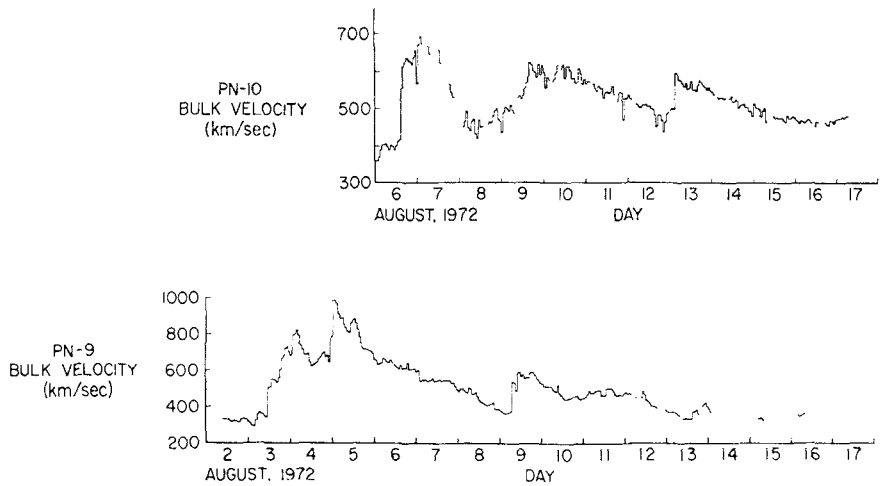

Fig. 3. Preliminary one-hour averages of velocity observed by Pioneer 10 at 2.2 AU and by Pioneer 9 at 0.77 AU during the August, 1972 disturbances (Dryer, 1974).

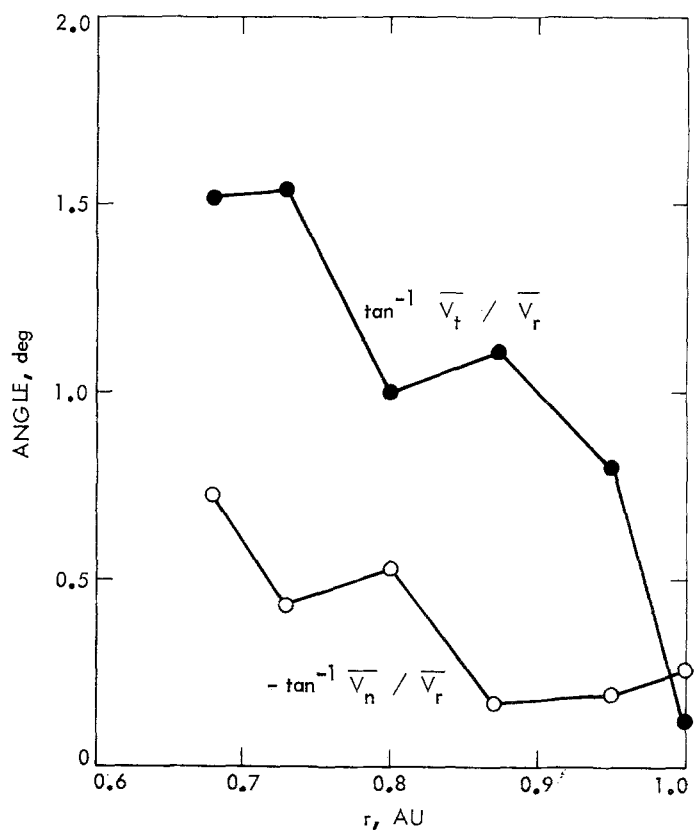

Fig. 4. Mariner-5 observations of the angles of solar-wind flow in (solid circles), and perpendicular to (open circles) the solar equator. The angles were computed from solar-rotation averages of the solar-wind velocity components (Lazarus and Goldstein, 1971).

2.2. Solar-wind direction

The only available analysis of the radial dependence of the solar-wind flow direction is by Lazarus and Goldstein (1971). Figure 4 shows the angles in and perpendicular to the solar equator as calculated from solar-rotation averages of the radial, tangential, and normal velocity components, V_r, V_t, and V_n, observed by Mariner 5 between

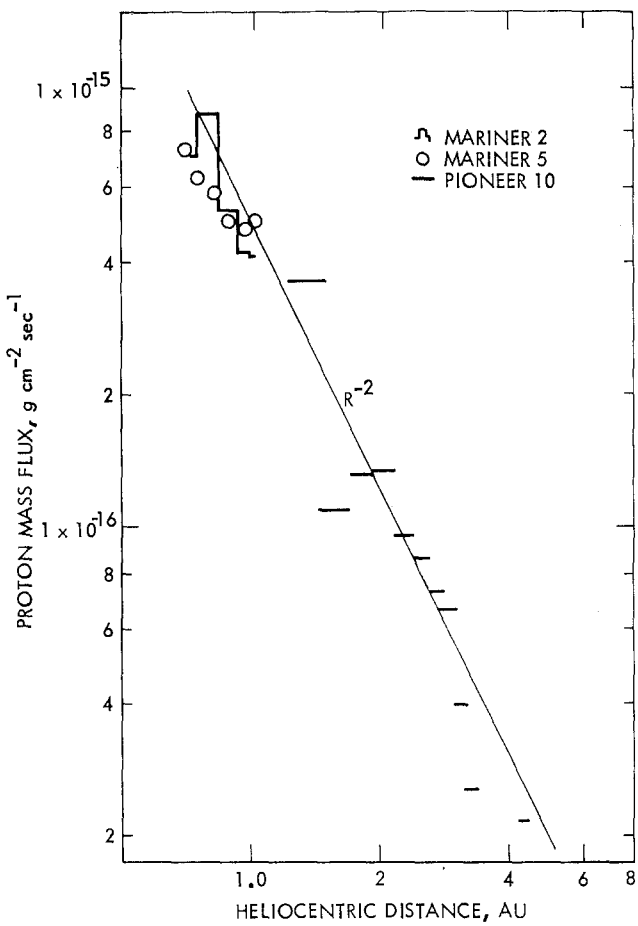

Fig. 5. Solar-rotation averages of the proton mass flux of the solar wind as a function of distance from the Sun.

June and November, 1967. The angle in the equatorial plane $\tan^{-1}(\langle V_t \rangle / \langle V_r \rangle)$, decreased from about 1.5° in the sense of corotation with the Sun at 0.7 AU to about 0.2° corotation at 1 AU. The angular momentum flux density was approximately constant between 0.7 and 1 AU and was consistent with earlier estimates deduced from comet tails (Brandt and Heise, 1970). The flow was consistently from north to south, toward the heliographic equator.

2.3. Mass flux

Figure 5 shows the radial dependence of solar-rotation averages of the proton mass flux (mass density times velocity) as observed by Mariner 2 in 1962 (Neugebauer and Snyder, 1966), by Mariner 5 in 1967 (Lazarus and Goldstein, 1971), and by Pioneer 10 in 1972 and 1973 (J. H. Wolfe, personal communication). The data are consistent with an inverse-square dependence of flux on radial distance as expected for spherically symmetric flow of the solar wind. Despite the variety of solar conditions and the use of three different instruments, all the solar-rotation averages in Figure 5 lie within a factor of 1.5 of 4×10^{-16} R^{-2} gm cm^{-2} s^{-1}, for the radial distance R in AU.

2.4. Temperatures

The horizontal bars in Figure 6 represent solar-rotation averages of the solar-wind proton temperature measured by Pioneer 10 as a function of its distance from the Sun (This figure is kindly provided in advance of its publication elsewhere by J. H. Wolfe). The temperatures were calculated by a least-squares fit of a convected isotropic Boltzmann distribution to measurements of flux as a function of energy/charge and direction. The bar plotted at 7×10^4 K contains data obtained during the August, 1972 events; this bar actually should be plotted off-scale at 1.28×10^5 K. The three lowest-temperature averages (near 3 AU) are lower limits to the true average temperatures for these rotations. The proton temperature evidently decreases more slowly

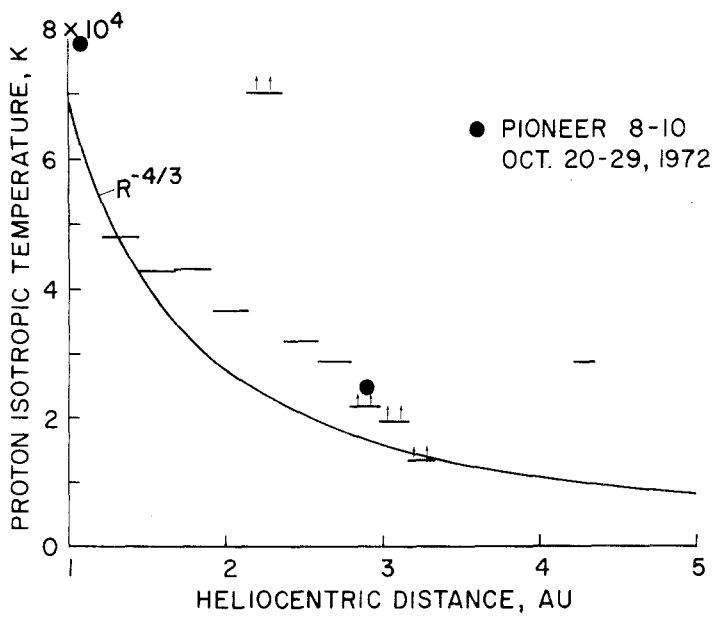

Fig. 6. Solar-rotation averages of proton temperatures observed by Pioneer 10 as a function of distance from the Sun. The circles represent simultaneous observations of proton temperatures by Pioneer 8 (near 1 AU) and Pioneer 10 (near 3 AU).

than $R^{-4/3}$, the radial dependence expected for adiabatic cooling. The circles in Figure 6 represent simultaneous temperature measurements by Pioneer 8 (near 1 AU) and Pioneer 10 (near 3 AU) when they were at approximately the same solar longitude. These two points yield a radial dependence of about $R^{-1.0}$.

There are few reports of observations of solar-wind electrons except near the Earth, where the average electron temperature is $\sim 1.5 \times 10^5$ K. The electron temperature is much less variable than the proton temperature, usually remaining between 1 and 2×10^5 K (Montgomery, 1972; Scudder *et al.*, 1973). Gringauz *et al.* (1973) report that near Mars, the solar-wind electron temperature did not exceed 5 to 8×10^4 K during the two months of intermittent solar-wind observations by Mars 3. If these measurements are representative of conditions at 1.52 AU, the electron temperature must decrease at least as fast as $R^{-1.5}$; i.e., the net electron temperature gradient between 1 and 1.52 AU must be even steeper than that associated with adiabatic expansion.

When the radial variations of the proton and electron temperatures are considered together, it is apparent that thermal energy must be transferred from the electrons to the protons. Gringauz *et al.* suggest that plasma instabilities play an important role. According to the data presented here, the sum of the electron and proton temperatures decreases roughly adiabatically, as would be expected for a collision-dominated fluid. The problems associated with understanding the transfer of energy between proton flow kinetic energy, proton and electron thermal energies, and electron heat conduction are far from being solved by these preliminary data from Pioneer 10 and Mars 3. More definitive results are eagerly awaited.

2.5. Magnetic field

Figures 7 and 8 summarize the observed radial dependence of the radial and tangential components of the interplanetary magnetic field. The periods of observation and the sources of the data are listed in Table II. The Mariner points were read from Coleman *et al.*'s (1969) and Rosenberg and Coleman's (1973) plots of running 27-day averages at intervals of approximately 27 days. Unfortunately, the data sets are not strictly comparable. In Figure 7, the Mariner-4 and -5 and the Pioneer-6 data are all solar-rotation averages of the magnitude of B_r, whereas each of the Pioneer-10 data points is the most-probable value of $|B_r|$ observed during a solar-rotation period. Comparison of the data in Figure 8 is further complicated by the fact that the Mariner data are

TABLE II

Sources of data in Figures 7 and 8

Spacecraft	Period of observations	Reference
Mariner 4	Nov. 64–July 65	Coleman *et al.* (1969)
Pioneer 6	Dec. 65–Sept. 66	Burlaga and Ness (1968)
Mariner 5	June 67–Nov. 67	Rosenberg and Coleman (1973)
Pioneer 10	March 72–Nov. 73	Smith (1974)

averages of the magnitude of the heliographic azimuthal component B_ϕ; the Pioneer-6 averages are of $\sqrt{B_\phi^2+B_\theta^2}$, the component of the field perpendicular to the radius vector; and the Pioneer-10 data are the most-probable values of $|B_\phi|$. Since the most-probable value of any field component is almost certainly less than the average of the magnitude of that component, the Pioneer-10 data in Figures 7 and 8 are expected to lie somewhat below the rest of the data, which is in fact observed.

With these cautions about data comparability in mind, one is led to conclude that

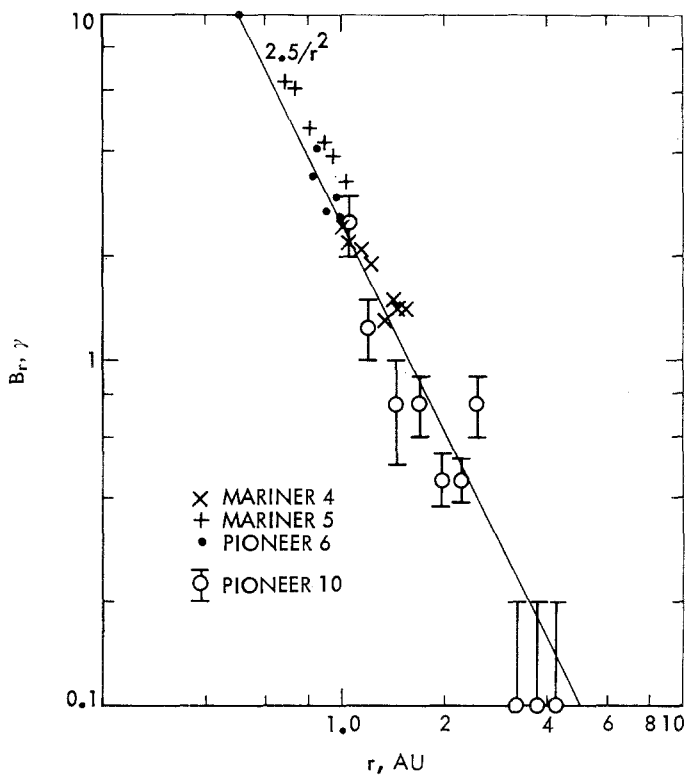

Fig. 7. Solar-rotation averages of the magnitude of the radial component of the magnetic field measured by Mariner 4, Mariner 5, and Pioneer 6, and the most-probable values of the magnitude of this component measured by Pioneer 10.

the B_r-data in Figure 7 can be well approximated by an inverse square dependence on heliocentric distance in agreement with Parker's spiral model (Parker, 1963). This conclusion disagrees with those of Coleman *et al.* (1969) who found an $R^{-1.46}$ dependence for the Mariner-4 data and Rosenberg and Coleman (1973) who found an $R^{-1.78}$ dependence for the Mariner-5 data. This disagreement is probably due to the unavoidable time variations.

The data in Figure 8 are harder to understand. The radial dependence of B_ϕ appears to be much steeper than the R^{-1} dependence expected for the Parker spiral model.

The observed small gradients of the radial and tangential components of the solar-wind velocity would tend to flatten rather than steepen the radial gradient of B_ϕ. The discrepancy cannot be entirely due to the difference between the most probable and the average values of $|B_\phi|$ and/or to the difference between B_ϕ and $\sqrt{B_\phi^2+B_\theta^2}$, because the gradient observed by each of the four spacecraft alone is steeper than R^{-1}. Coleman *et al.* (1969) obtain an average dependence of $R^{-1.29}$ for Mariner 4; Rosenberg and Coleman (1973) compute a best fit of $R^{-1.85}$ for Mariner 5, and the Pioneer-6

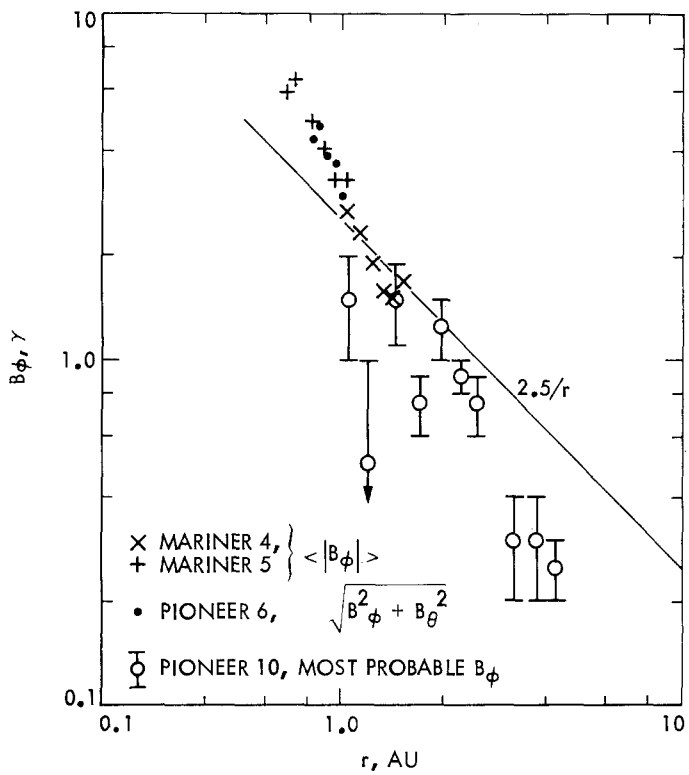

Fig. 8. Solar-rotation averages of the magnitude of the azimuthal component of the magnetic field measured by Mariners 4 and 5, averages of the magnitude of the field component perpendicular to the radius vector measured by Pioneer 6, and the most-probable values of the magnitude of the azimuthal field measured by Pioneer 10.

and Pioneer-10 data plotted in Figure 8 yield dependences of $R^{-1.9}$ and $R^{-1.1}$, respectively. The Pioneer-10 value, which is based on the most-probable, rather than the average, values of $|B_\phi|$, comes closest to agreement with the theoretical spiral. In Figure 9, which shows histograms of Pioneer-10 field directions at 1.04 and 4.3 AU, it is seen that the spiral angle is still well defined at 4.3 AU, with a most-probable value near 100°. Extrapolation of the Mariner-4 and -5 results to 4.3 AU yields field angles of 126° and 140°, respectively. Figure 10 shows the most-probable Pioneer-10

field angles for each solar rotation plotted as a function of heliocentric distance, together with the theoretical spiral angles for a solar-wind velocity of 360 km s^{-1}. The short curves marked M4 and M5 are the least-squares fits to the Mariner-4 and -5 data. Although the Pioneer-10 data lie close to the theoretical spiral, there are many short-term excursions greater than those corresponding to the Mariner data. We are left with a choice of conclusions: either (1) B_ϕ drops off faster with distance from the Sun than predicted by Parker's spiral model, (2) time variations from one solar rota-

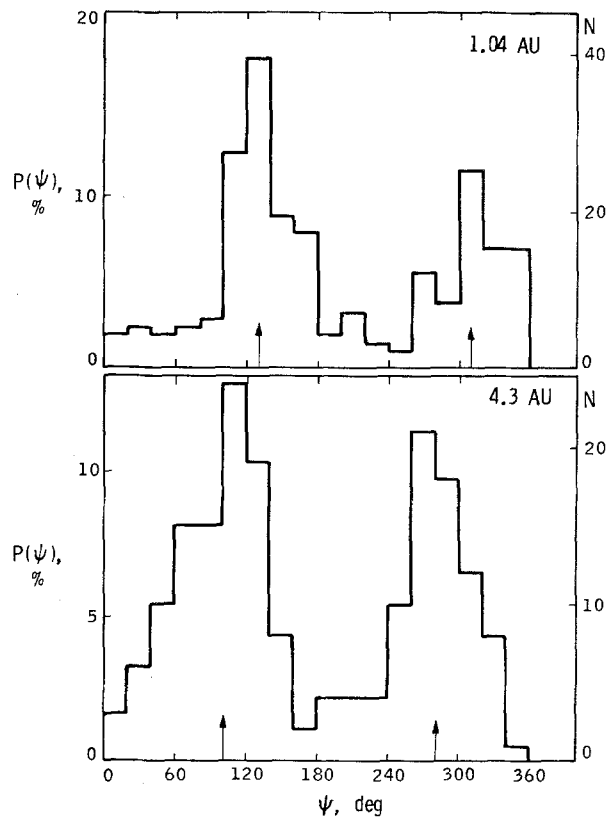

Fig. 9. Solar-rotation histograms (three-hour averages) of the direction of the interplanetary magnetic field as observed by Pioneer 10 at 1.04 and 4.3 AU.

tion to the next happened to be in such a sense to give steeper-than-average gradients of B_ϕ for Mariners 4 and 5 and Pioneer 6, or (3) the most-probable values of $|B_\phi|$ and the field direction are the correct parameters to analyze due to the distortion of the average values by fluctuations.

2.6. Fluctuations

Figure 11 shows the observed radial variations of fluctuations in both the radial

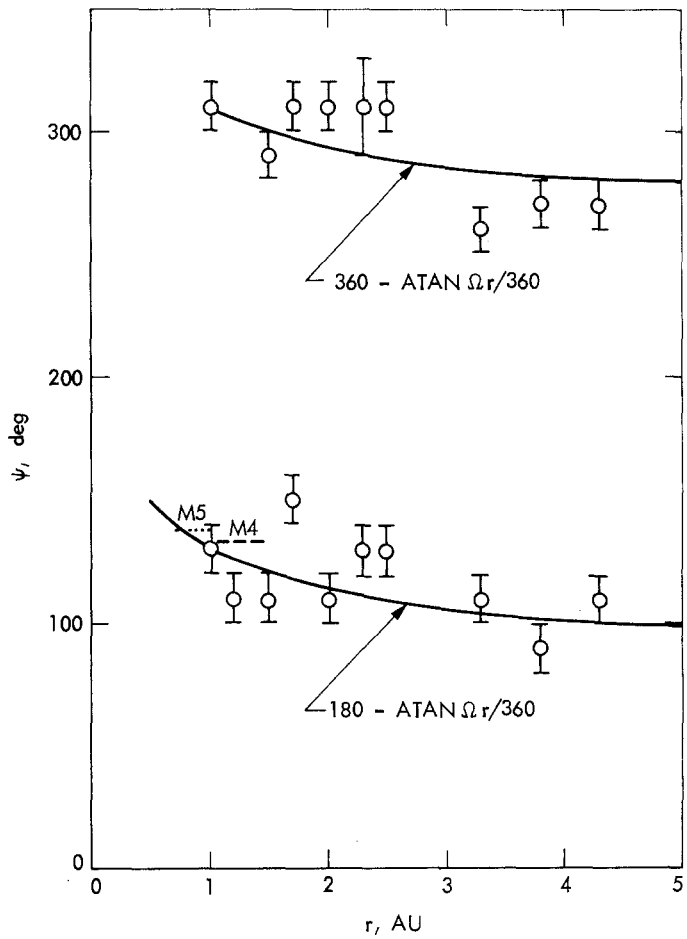

Fig. 10. Radial variation of the most-probable values of the direction of the interplanetary magnetic field observed by Pioneer 10 during a solar rotation. The short curves labeled M4 and M5 are the best fits to this angle computed from the Mariner-4 and -5 data. The long curves are the angles corresponding to the Parker spiral model for a solar-wind velocity of 360 km s^{-1}.

component and the magnitude of the interplanetary magnetic field. The Mariner-4 data are the best fits of the form $\sigma = C\,R^{-k}$, where σ is the 27-day average of the daily rms deviation of the quantity considered (see Coleman *et al.* (1969) for details). The Mariner-5 data were read from curves (Rosenberg and Coleman, 1974) of running 27-day averages of the daily rms deviations at intervals of approximately 27 days. The Pioneer-10 data are the most-probable (on a logarithmic scale) daily variances for each solar rotation.

For both Mariners 4 and 5 and for Pioneer 10 the power in the fluctuations in each of the three components B_r, B_ϕ, and B_θ, were roughly equal to each other and a factor of 2 to 5 greater than the power in the magnitude variations. Thus, at all radial distances sampled, variations in field direction are more important than variations in

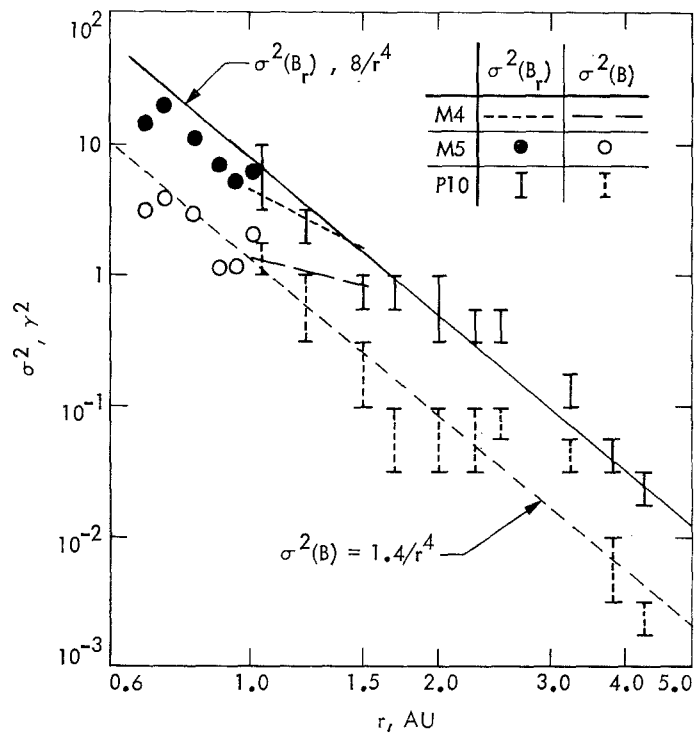

Fig. 11. Variances of the magnitude and radial component of the interplanetary magnetic field as a function of heliocentric distance. The Mariner data are solar-rotation averages of the daily rms deviations, while the Pioneer-10 data are most-probable values of the daily variances.

field magnitude. The data from the three spacecraft are in rough agreement with each other despite the different methods of calculation.

The Pioneer-10 observation that $\sigma^2(B_r)$ decreases as R^{-4} while B_r decreases as R^{-2} implies that $\Delta B_r/B_r$ is roughly independent of distance from the Sun. However, the Mariner-5 results indicate an increase in $\Delta B/B$ between 1 and 1.5 AU roughly proportional to $R^{0.7}$ (Coleman *et al.*, 1969). Parker (1965) and Dessler (1967) predict that $\Delta B/B$ for undamped waves would increase with distance from the Sun up to a shock-limited ratio $\Delta B/B = 1$, which Coleman *et al.* (1969) suggest may occur at about 4.3 AU.

Changes in the spiral angle of the field are related to temporal and spatial changes in the velocity of the solar wind (Schatten, 1971). The Pioneer-10 results show that large scale velocity variations die out with increasing radial distance from the Sun; this damping of velocity variations may thus slow the rate of increase of $\Delta B/B$ with distance.

Intriligator's (1974b, 1974c) studies of density fluctuations along the Pioneer-10 trajectory shows that the slope of the density power spectrum between 10^{-3} and 10^{-4} Hz remains essentially unchanged between 1 and 3 AU, while the power level decreases by an order of magnitude.

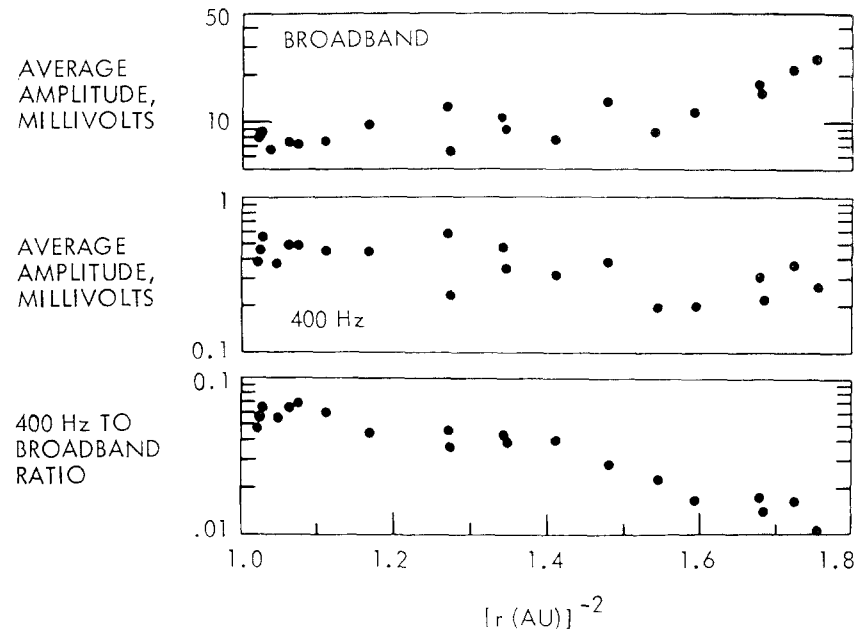

Fig. 12. Average broadband and 400 Hz readings for twenty VLF events observed by Pioneer 9 (Scarf *et al.*, 1973).

Scarf *et al.* (1973) analyze 20 periods of enhanced VLF electric-field emission observed by Pioneer 9 between 0.75 and 1 AU. Their results, shown in Figure 12, indicate a significant radial gradient in the emission observed in the two low frequency channels of the instrument. Figure 13 shows two simple models of the spectrum of this enhanced emission; each model fits some of the Pioneer-9 observations. Since later observations by Pioneer 9 during the August, 1972 events show a clear relation between broadband emission and the proton density and proton plasma frequency f_p^+ (Scarf and Wolfe, 1974), case 2 in Figure 13 is probably the better model and the emissions are probably related to ion acoustic oscillations.

Two studies have been made of the radial variation of the rate of occurrence of discontinuities in the interplanetary magnetic field. Using Pioneer-6 data, Burlaga (1971) finds rates of 0.7 discontinuities per hour near 0.82 AU, 0.8 h^{-1} near 0.91 AU, and 1.1 h^{-1} near 0.98 AU. The author warns, however, that the gradient may not be real, but an artifact arising from better data acquisition near 1 AU. On the other hand, Mariani *et al.* (1973) find a possible inverse relation between radial distance and the occurrence rate of discontinuities observed by Pioneer 8. These data are plotted in the middle panel of Figure 14. An extrapolation of the linear best fit predicts the disappearance of all discontinuities at 1.2 AU; Mariner-4 and Pioneer-10 data prove otherwise. The bottom panel of Figure 14 shows an alternate interpretation of the data as a heliographic latitude effect. We conclude that the radial variation of the occurrence rate of discontinuities is not yet firmly established, and move on to a discussion of other possible latitude dependencies.

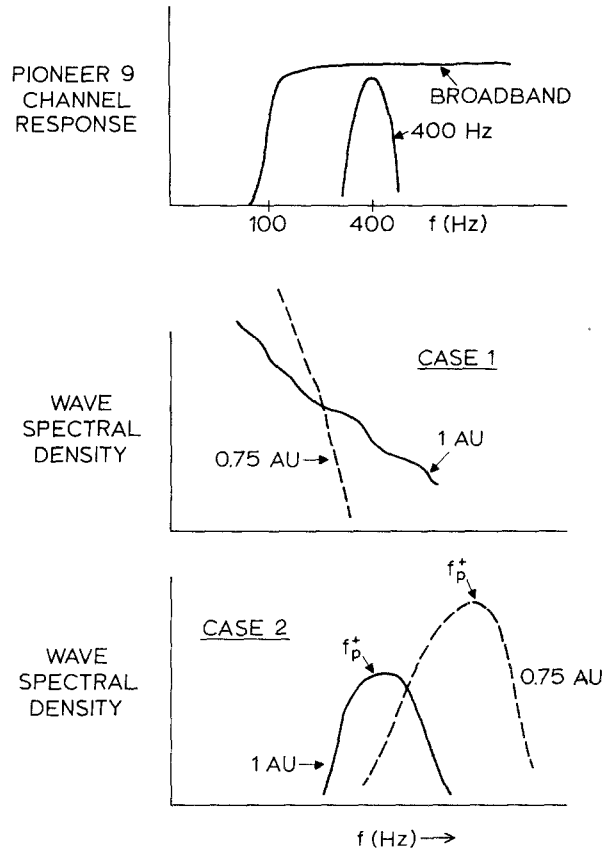

Fig. 13. Frequency response of the broadband and 400 Hz channels of the Pioneer 9 VLF electric-field detector and two models of the interplanetary wave spectrum used to explain the radial variations shown in Figure 12 (Scarf *et al.*, 1973).

3. Latitudinal Gradients

To date, all spaceprobe observations have been limited to near the ecliptic plane. But the 7°15′ inclination of the ecliptic to the solar equator allows observations of the properties of the solar wind over the heliographic latitude range $\pm 7.25°$. The large amplitude of some observed latitude effects is thus somewhat surprising because most visible solar activity occurs at higher latitudes.

3.1. Solar-wind velocity

The first in situ observations of a dependence of solar-wind velocity on heliographic latitude were obtained from a study of five years of data from the Vela satellites (Hundhausen *et al.*, 1971). Figure 15 shows the results of this analysis. From bottom to top, this figure shows: the heliographic latitude of the Vela satellites, the number of Vela-3 or -4 observations per solar rotation, the average solar-wind velocity for each solar rotation, and the average proton density for each solar rotation observed by

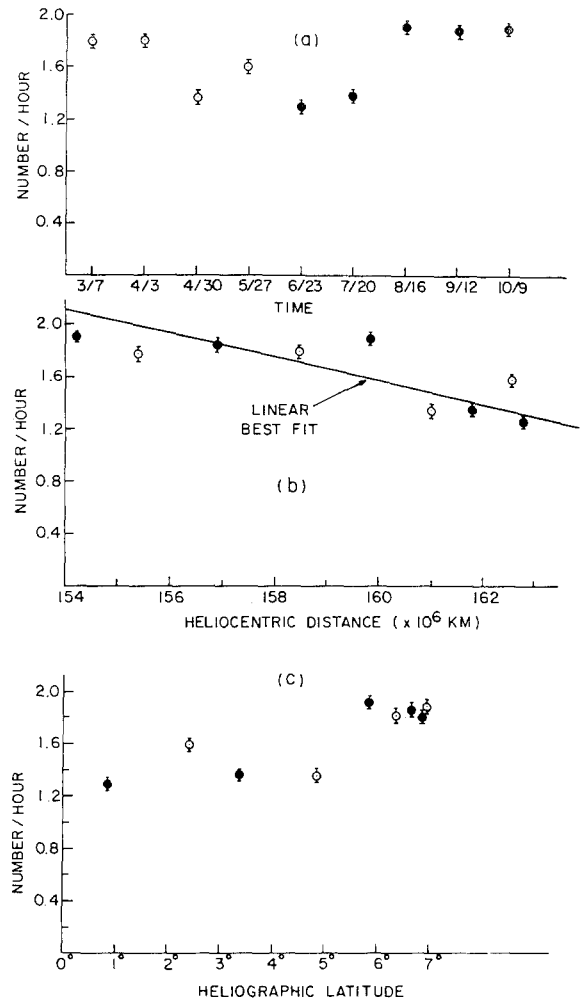

Fig. 14. Apparent dependence of solar-rotation averages of the occurrence rate of discontinuities in the interplanetary magnetic field on (top) time, (middle) distance from the Sun, and (bottom) heliographic latitude (Mariani *et al.*, 1973).

Vela 3 and 4. The arrows at the top of the figure denote the times of crossing the solar equator. During 1965 and 1966, the velocity apparently varied with latitude, reaching a minimum near the equator and a maximum value 50 to 150 km s^{-1} greater at latitudes of $\pm 7°$. The peak velocity in the northern hemisphere was consistently greater than that in the southern. The difference in average velocity is due to the more frequent occurrence of high-speed streams at the higher latitudes. The disappearance of the effect in late 1967 and early 1968, when the velocity essentially remained in its high-latitude state, is probably related to solar-cycle effects. All latitude variations of the plasma properties directly observed between $\pm 7°$ were in this interval at the start of a new solar cycle. Hundhausen *et al.* (1971) suggest that this near-

equatorial latitude variation may be limited to this period of most rapid migration of active centers from high to low latitudes.

Rhodes and Smith (1973, 1974) and Smith and Rhodes (1974) also find a latitudinal gradient in a comparison of Mariner-5 data with near-Earth data obtained by Explorers 33, 34, and 35. Some of their results are shown in Figure 16, which is a plot of the difference between the hourly average velocity V_E observed at the Explorers

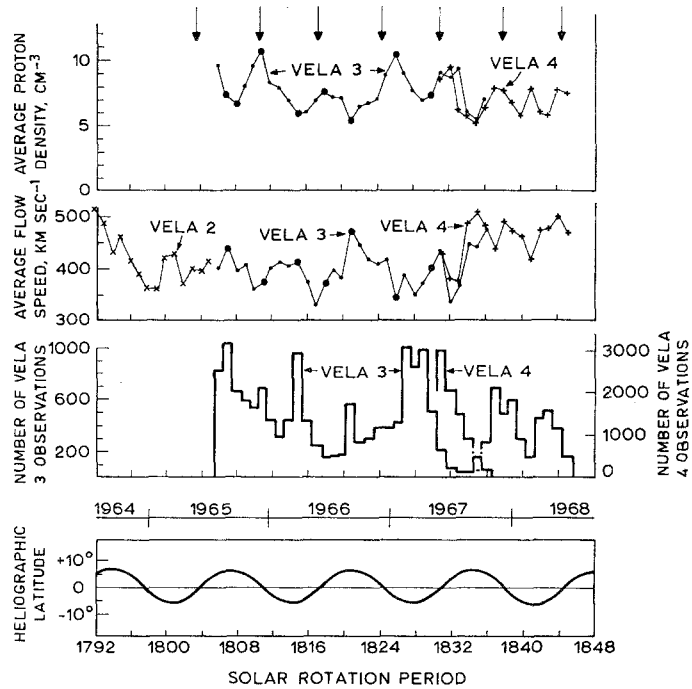

Fig. 15. Vela observations of solar-rotation averages of proton density and velocity together with the number of Vela observations in each solar rotation and the heliographic latitude of the observations.

and the velocity V_M observed at Mariner 5 an expected transit time earlier vs the difference in the latitudes of the two spacecraft. The error bars in Figure 16 are standard deviations. The least-squares linear fit to the data is represented by the double line with a slope of 15 km s^{-1} deg^{-1}. These observations were made during the period June–November, 1967, when the Vela satellites still observed a latitudinal variations, but with a slight shift in phase relative to 1965 and 1966. The magnitude of the latitudinal velocity gradient found by the Mariner-Explorer comparison agrees well with that observed by Vela; both of these direct measurements between $\pm 7°$ give a steeper gradient than that deduced from interplanetary scintillation (IPS) observations over a much greater range of latitudes.

Figure 17, from Coles and Maagoe (1972), shows the velocity computed from IPS measurements as a function of the solar latitude of the dominant scattering region. The observations were made from March to June, 1972. The Rhodes and Smith

gradient of 15 km s^{-1} deg^{-1}, indicated by the straight line in Figure 17, is somewhat steeper than the rate of change with latitude of the velocity calculated from the IPS data. The IPS data are consistent with some of the smaller velocity variations seen by the Vela satellites in 1965.

Coles *et al.* (1974) discuss the latitude dependence calculated from a large number of IPS observations in 1973. They find that the average velocity increases systemati-

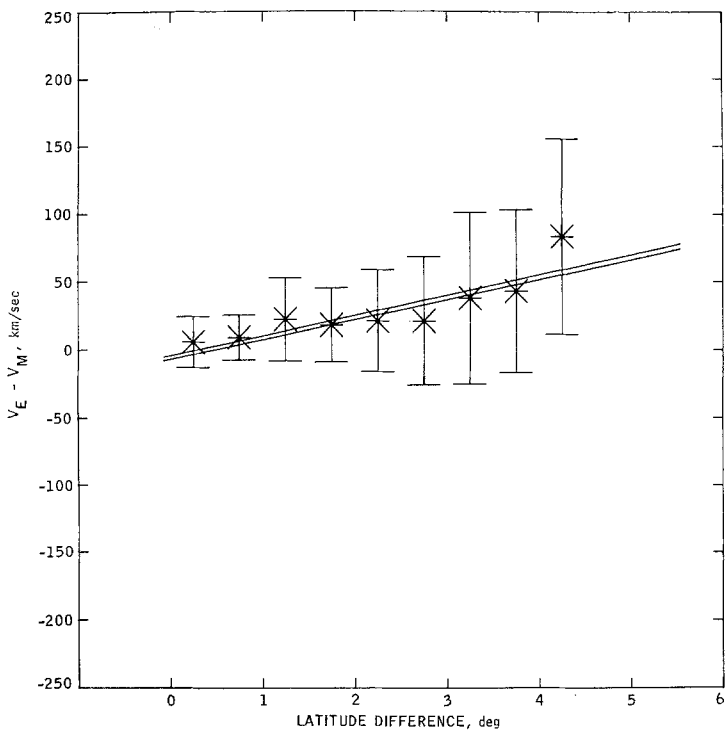

Fig. 16. The difference between the solar-wind velocities observed near the Earth, V_E, and at Mariner 5, V_M, averaged over 0.5° intervals of the difference between the Earth's and Mariner's solar latitudes (Rhodes and Smith, 1974b).

cally from 400 km s^{-1} at the equator to 550 km s^{-1} at $\pm 70°$, which corresponds to an average gradient of 2.1 km s^{-1} deg^{-1}.

3.2. Other plasma parameters

Many of those solar-wind parameters which generally correlate (anticorrelate) with velocity show the same (opposite) latitude dependence as the velocity during the rising part of the present solar cycle. Most notably, the well known anticorrelation of solar-wind density and velocity is clearly apparent in Figure 15. Note, however, that the latitude variation of density had a smaller north-south asymmetry than the velocity.

The ratio of the number density of alpha particles to that of protons, n_α/n_p, cor-

relates well with the solar-wind velocity (Hirshberg *et al.*, 1972; Ogilvie, 1972; Bollea *et al.*, 1972; Moreno and Palmiotto, 1973; Ogilvie and Hirshberg, 1974). Figure 18, from Robbins *et al.* (1970), shows solar-rotation averages of this ratio observed by the Vela-3 satellites from July, 1965 to July, 1967. Close comparison of Figures 18 and 15 reveals a strong correlation between n_α/n_p and velocity and between n_α/n_p and solar latitude. This association was pointed out by Rosenberg *et al.* (1971).

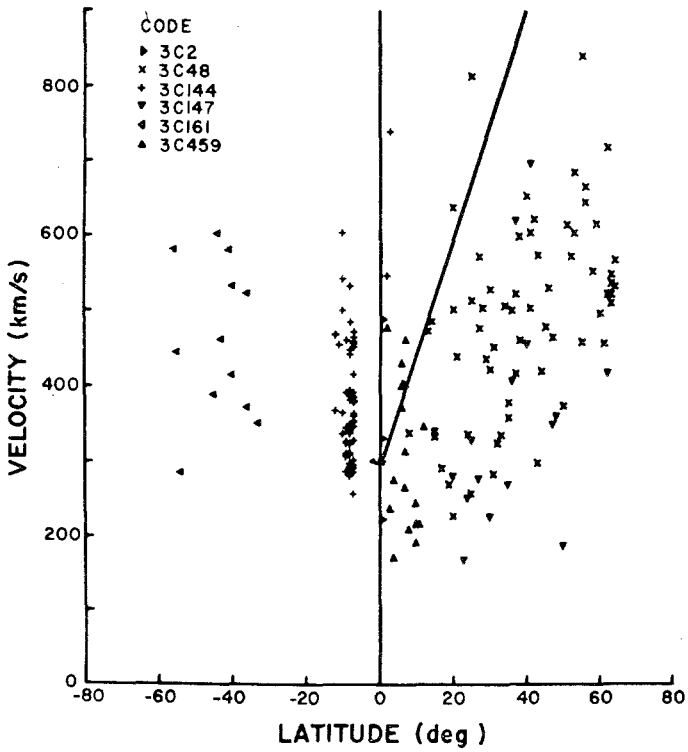

Fig. 17. Solar-wind velocity calculated from observations of interplanetary scintillations as a function of the solar latitude of the dominant scattering region (Coles and Maagoe, 1972). A straight line has been added to the Coles and Maagoe data to indicate the slope of the latitudinal variation found by Rhodes and Smith during a different art of the solar-activity cycle.

The direction of flow in the solar equatorial plane also correlates with the solar-wind velocity (Coon, 1968; Lazarus, 1970; Hundhausen *et al.*, 1970). At low velocities, the flow shows more corotation with the Sun; i.e., it comes from further east. Figure 19 (Strong *et al.*, 1967) shows the time variation of solar-rotation averages of the flow direction measured by the Vela-2 satellites from July, 1964 to July, 1965. Comparison of Figures 19 and 15 shows that the most eastward flow occurred during rotations 1798 and 1805, which are within one rotation of the equator crossing. The most nearly radial flow was observed during rotations 1794 and 1800, when the solar latitude was large. Egidi and Signorini (1974) show daily averages of the flow direction observed

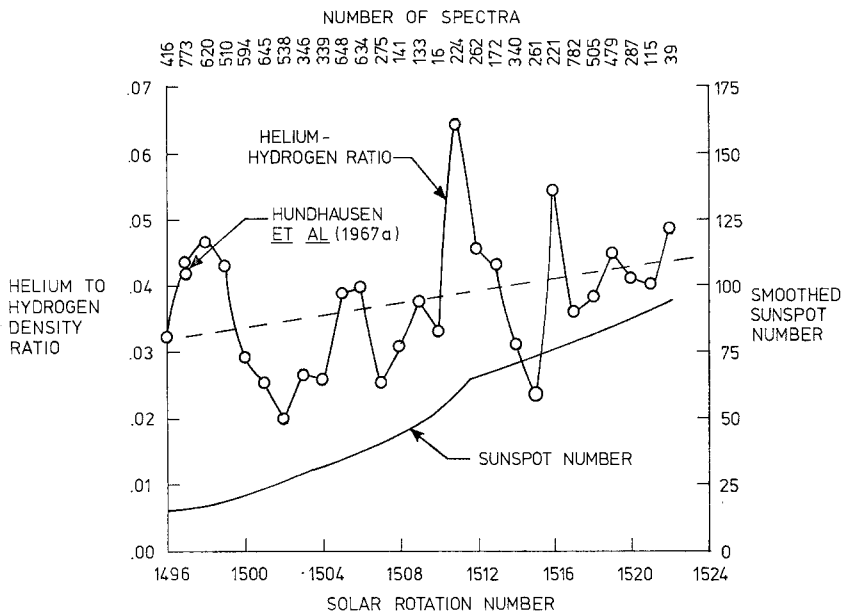

Fig. 18. Time variation of solar-rotation averages of the ratio of the number density of helium to that of hydrogen observed by Vela 3 during the period July, 1965 to July, 1967 (Robbins *et al.*, 1970).

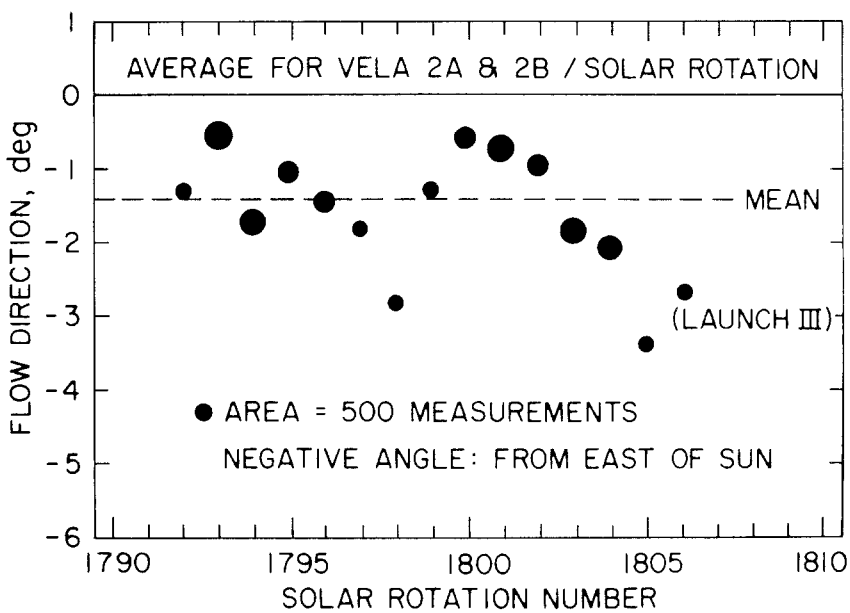

Fig. 19. Time variation of solar-rotation averages of the solar-wind flow direction (in a plane close to the ecliptic) observed by Vela 2 from July, 1964 to July, 1965 (Strong *et al.*, 1967).

by Explorer 33 and Heos 1 during the years 1967–1971. No latitude or seasonal effect is obvious in these later data.

3.3. Magnetic field

The interplanetary magnetic field also showed latitude dependencies during the early part of the present solar cycle.

Figure 20 is an extension by Wilcox (1970) of a figure originally published by Rosenberg and Coleman (1969). It shows that from 1964 through 1967, there was a strong latitude control of the fraction of the time that the interplanetary magnetic field had a negative polarity (inward, toward the Sun). The latitude modulations of the polarity and the solar-wind velocity both ceased in late 1967. An analysis of geomagnetic data from the years 1926–1971 shows that this disappearance is a solar-cycle effect and that the latitude modulation of the field polarity will probably return, with oppo-

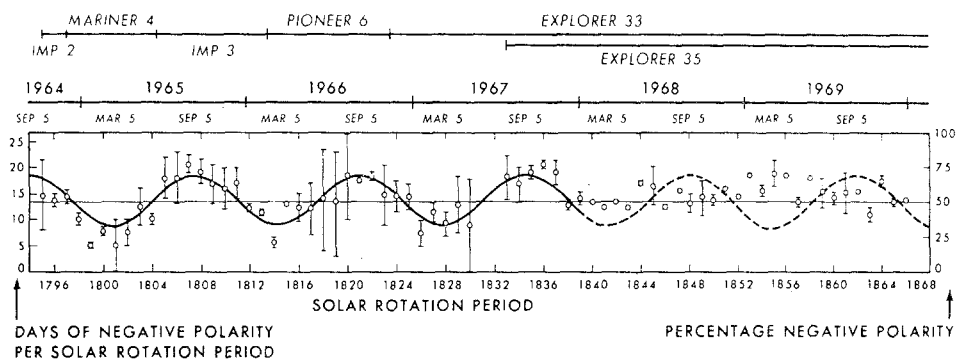

Fig. 20. Solar-rotation averages of the percentage of the time the interplanetary magnetic field has negative polarity (Wilcox, 1970).

site phase, after the solar polar magnetic field has completed its reversal (Wilcox and Scherrer, 1972).

The θ-component of the interplanetary magnetic field depends on whether the observation is made north or south of the equator. Figure 21 (after Coleman and Rosenberg, 1971) shows this effect in the Mariner-4 data obtained in 1964 and 1965. The + symbol in the top panel gives the 27-day average (computed every 3 days) of B_θ when the polarity of the interplanetary magnetic field is positive (outward from the Sun). The bottom part of Figure 21 shows a model of the skewing of the field lines which is consistent with the magnetic data. During most of the interval shown in Figure 21, Mariner 4 was south of the equator, so B_θ for positive polarity should have been, and was, positive. The generally negative values of B_θ for negative polarity, represented by dots in the top of Figure 21, is also in agreement with the model. Both $B_{\theta+}$ and $B_{\theta-}$ changed sign when Mariner 4 crossed the equator, as expected. The reality and persistence of the effect for periods of low and moderate activity are verified by analyses of the data from Mariners 2 and 5 (Coleman and Rosenberg,

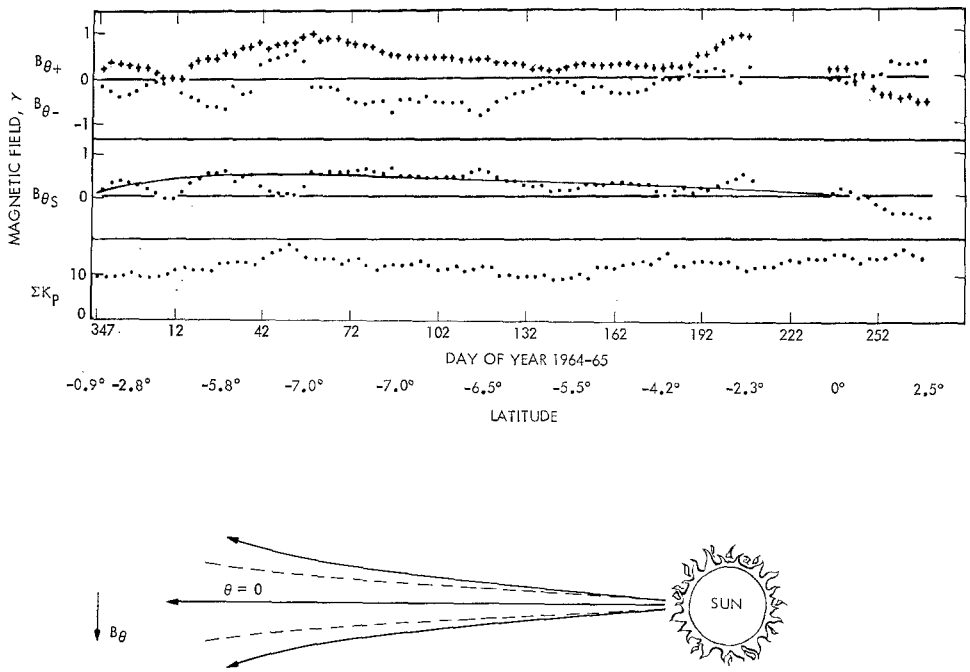

Fig. 21. (Top) Running 27-day averages of $B_{\theta+}$ (the value of B_θ when the field polarity is positive) and $B_{\theta-}$, $B_{\theta S}=0.5\ (B_{\theta+}-B_{\theta-})$, and the daily geomagnetic index ΣK_p for Mariner 4. (Coleman and Rosenberg, 1971). (Bottom) A simple model consistent with the observed skewing of the interplanetary magnetic field.

1971), Explorers 33 and 35 (Rosenberg *et al.*, 1971), and Imp 3, Pioneer 6, and Explorer 34 (Rosenberg *et al.*, 1973).

From the model drawn in the bottom of Figure 21, Coleman and Rosenberg (1971) predict that the streamlines of the solar-wind flow would be along the field lines and that the solar-wind velocity would have an average component away from the equator. The Mariner-4 and -5 velocity data show the opposite to be true; i.e., the solar wind usually flowed toward the equator. To resolve this discrepancy, Coleman and Rosenberg suggest that the field-velocity relation may be controlled by a 'standing Alfvén disturbance'.

4. Solar-Cycle Effects

Since both cosmic-ray intensity and geomagnetic activity show strong solar-cycle variations, and since the solar wind with its magnetic field is the principal link between the Sun and cosmic rays and between the Sun and the geomagnetic field, it has long been supposed that the properties of the solar wind must show significant solar-cycle variations. Such variations turn out to be subtle and hard to discern; most, if not all, solar-cycle variations are smaller than the day-to-day and solar rotation-to-solar rotation variations. Also, the search for solar-cycle variations of solar-wind properties must be limited to the analysis of data averaged over periods of six months,

or a multiple of six months, to avoid contamination by the latitude variations discussed in the last section.

The present solar-activity cycle, number 20, started with sunspot minimum in October, 1964. The sunspot number then rose to a broad, flat maximum which lasted for almost the entire three years 1968–1970. Both the 5303 Å coronal intensity and the yearly average of the geomagnetic K_p index peaked in 1968, whereas the occurrence rate of sudden commencement storms peaked in 1970.

4.1. Solar-wind velocity

Several people have published yearly averages of the solar-wind velocity, with the widely differing results shown in Figure 22. The yearly-average sunspot numbers are plotted at the top of the figure. The different line codes for the yearly-averages of

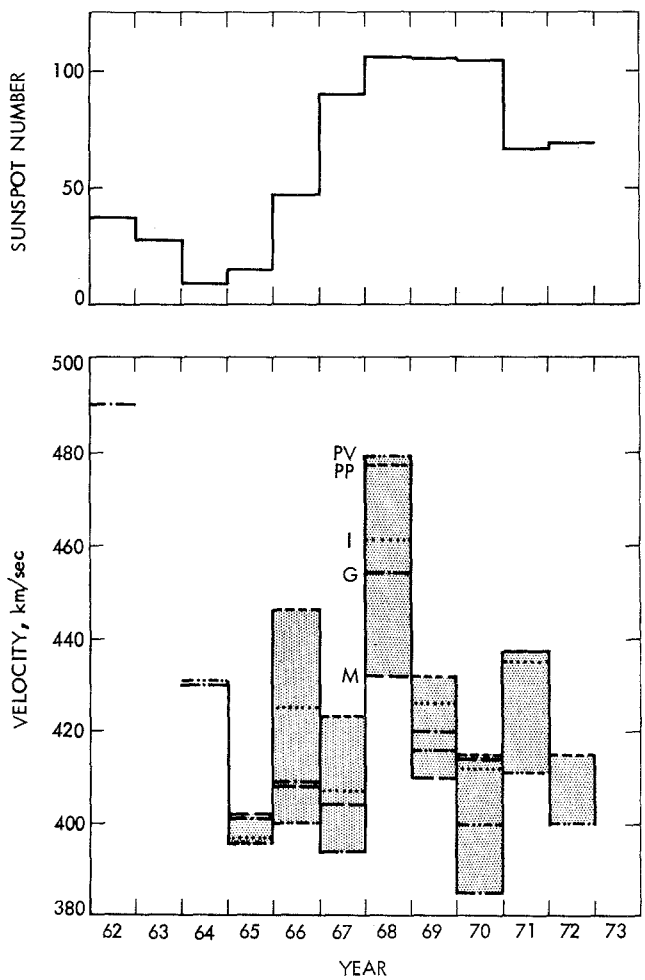

Fig. 22. (Top) Yearly averages of the sunspot number. (Bottom) Yearly averages of solar wind velocity. See Table III for the interpretation of the five types of line coding.

TABLE III

Sources of data in Figure 22

Symbol	Spacecraft	Years	Reference
G	Mariner 2 Vela 2, 3, 4, 5 Pioneer 6, 7	1962–1970	Gosling *et al.* (1971)
I	Vela 3, 4, 5 Pioneer 6, 7	1965–1971	Intriligator (1974a)
PV	Vela 2, 3, 4, 5	1964–1972	Pinter (1974)
PP	Pioneer 6	1966–1972	Pinter (1974)
M	Vela 3 Explorer 33, 34, 35 Heos 1	1965–1971	Diodato *et al.* (1974)

solar-wind velocity plotted at the bottom of the figure refer to the sources of the calculations; Table III gives information about these sources. The calculations of Diodato *et al.* (1974) differ from the others in that they have normalized all spacecraft to Vela 3 to correct for differences between the calibrations of the several instruments. The shading in Figure 22 extends from the lowest to the highest estimate of the velocity for each year. The temporal variations of the yearly-average velocity appear to be close to random, with the only obvious relation to solar activity being the high velocity observed in 1968.

It may be some property of the variation of velocity other than its mean which is important for cosmic-ray and geomagnetic effects. For example, Hirshberg (1973) has analyzed the solar-cycle variation of the distribution and the modal value of velocity. However, these parameters are very difficult parameter to work with because many velocity histograms have multiple peaks, some of which correlate with the centers of the instrument velocity channels. Figure 1 in Gosling *et al.* (1972) shows this effect very strongly in the Mariner-2 data. This is a very common problem except for the few instruments with very closely spaced velocity channels.

Figure 23 shows plots of six-month averages of the fraction of the time the solar-wind velocity exceeded 500 km s^{-1}. The notation used and the sources of the data are: M2 is Mariner 2 (available from the National Space Science Data Center); I1 is Imp 1 (Olbert, 1968); V2 is Vela 2 (Strong *et al.*, 1967); V3 is Vela 3 (Bame *et al.*, 1970); V is a combination of Velas (Obayashi, 1968); P6 and P7 are the MIT experiments on Pioneers 6 and 7 (Lazarus *et al.*, 1973); E33 and E35 are Explorers 33 and 35 (Diodato *et al.*, 1974); E34 is Explorer 34 (data courtesy of K. W. Ogilvie); H1 is Heos 1 (Diodato *et al.*, 1974), A15 is the Apollo-15 ALSEP (data furnished by D. R. Clay, B. E. Goldstein, M. Neugebauer, and C. W. Snyder); and the DM are two-year, normalized, multi-spacecraft distributions computed by Diodato and Moreno (1974). The Mariner-2 and Imp-1 values are necessarily shorter than 6 months. The Heos-1 data cover the periods December, 1968 to April, 1969 and August, 1969 to January, 1970. The principal messages in this complicated figure are (1) that the general trend of freq ($V > 500$ km s^{-1}) is similar to that of $\langle V \rangle$, and (2) that the long-term variation

of the solar-wind velocity is much more highly structured than most indices of solar activity, such as sunspot number. Figure 23 shows three local maxima, in late 1966, late 1968, and early 1971. There is a very deep minimum in early 1967, which is related to the relatively low average velocity shown for 1967 in Figure 22.

If the solar-wind velocity is basically responsible for the solar-cycle variations of cosmic rays and geomagnetic activity, the relevant parameter must be something other

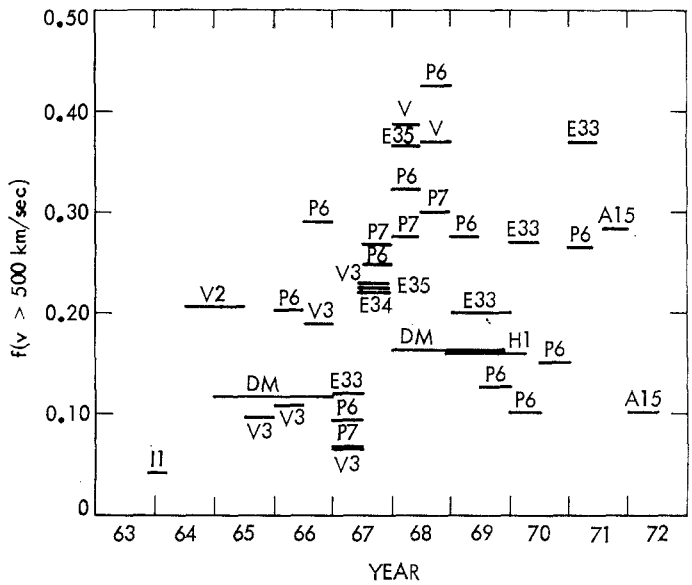

Fig. 23. Fraction of the time the solar-wind velocity was observed to be greater than 500 km s^{-1}. See text for meaning of symbols and sources of data.

than those already discussed. Intriligator (1974a) finds a correlation between the solar-wind stream structure and solar activity. Figure 24 shows the number of high-velocity streams observed per year and the number of days per year of high-speed streams. The solar-cycle effect is exaggerated in this figure, however, because there were fewer days of observation in 1965 and 1971 than in 1966–1970.

The year 1967 is somewhat of a mystery. All solar-wind parameters in Figures 22–24 show a local minimum then, whereas all the solar and geomagnetic indices listed at the start of this section, except for the number of storm sudden commencements, show a smooth rise across 1967.

4.2. Solar-wind density

Figure 25, from Diodato *et al.* (1974), summarizes much of the available data concerning the solar-cycle variation of proton density in the solar wind. They also compute the yearly-average densities from Vela 3, Explorers 33, 34, and 35, and Heos 1, all normalized to Vela 3; the results are given in Table IV. Diodato *et al.* conclude

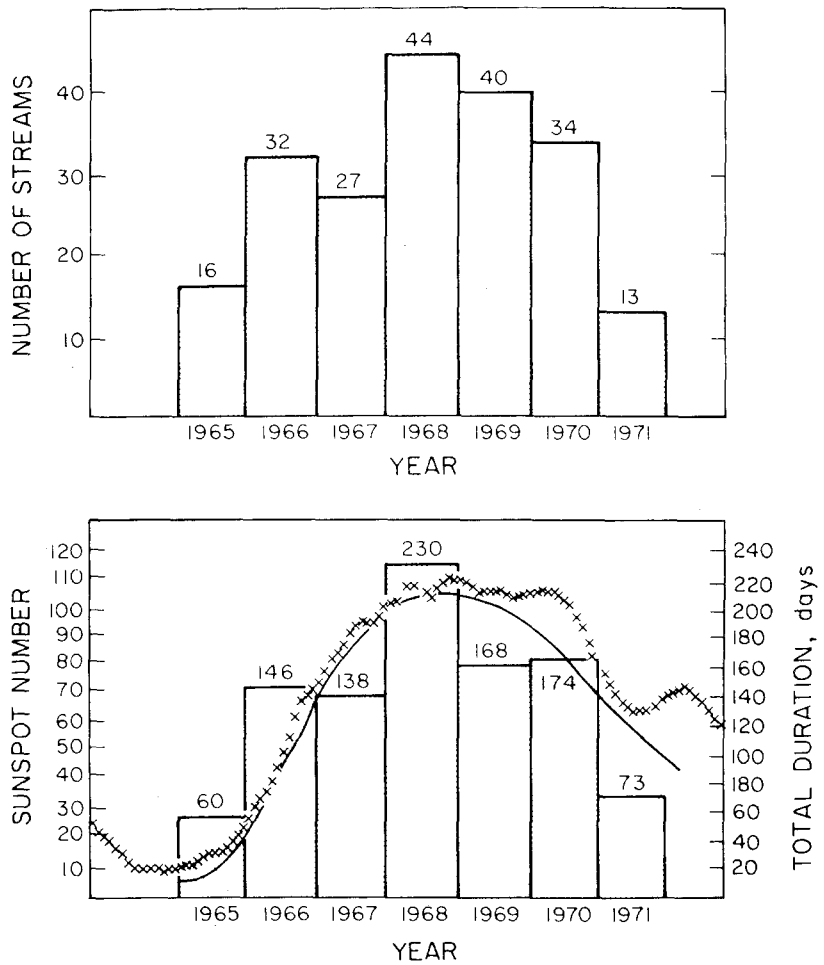

Fig. 24. (Top) The number of high-speed streams per year. (Bottom) The total duration, in days, of high-speed streams. The smooth curve and the crosses are the smoothed and measured sunspot numbers. (Intriligator, 1974a).

that there is a 50% modulation of the proton density which is anticorrelated with solar activity.

Figure 26 shows six-month averages of the fraction of the time that the proton density in the solar wind is greater than 10 cm^{-3}. The coding and data sources are the same as for Figure 23. The analysis is limited to data obtained near 1 AU. Except for 1967, a smooth anticorrelation with solar activity can be discerned, in agreement with Diodato *et al.* (1974).

4.3. Proton Temperature

Burlaga and Ogilvie (1970) and Hundhausen *et al.* (1970) show that, on the time scale of several solar rotations, the square root of the proton temperature is directly propor-

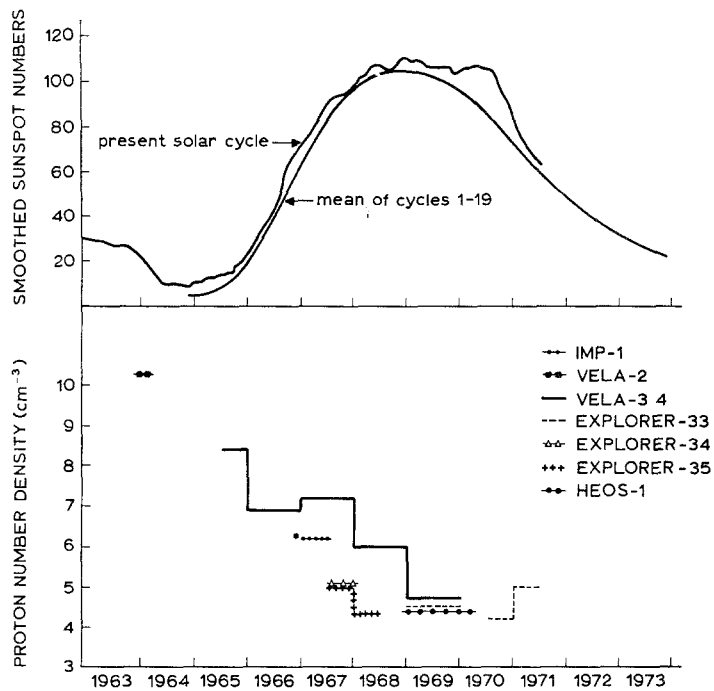

Fig. 25. Time variation of (top) sunspot numbers, and (bottom) average proton density in the solar wind (Diodato *et al.*, 1974).

TABLE IV

Yearly average proton density from 5 spacecraft, normalized to Vela 3. (From Diodato *et al.*, 1974)

Year	Density, cm^{-3}
1965	8.4
1966	7.0
1967	6.9
1968	5.6
1969	6.0
1970	6.6
1971	6.3

tional to the solar-wind speed. Table V gives the coefficients of least-squares fits to this relation computed for three different times between 1965 and 1971 by Burlaga and Ogilvie (1973); the coefficients are seen to be independent of the phase of the solar cycle.

4.4. Helium

The suggestion that the ratio of the number densities of helium to hydrogen in the solar wind correlates with the solar-activity cycle was first made by Robbins *et al.*

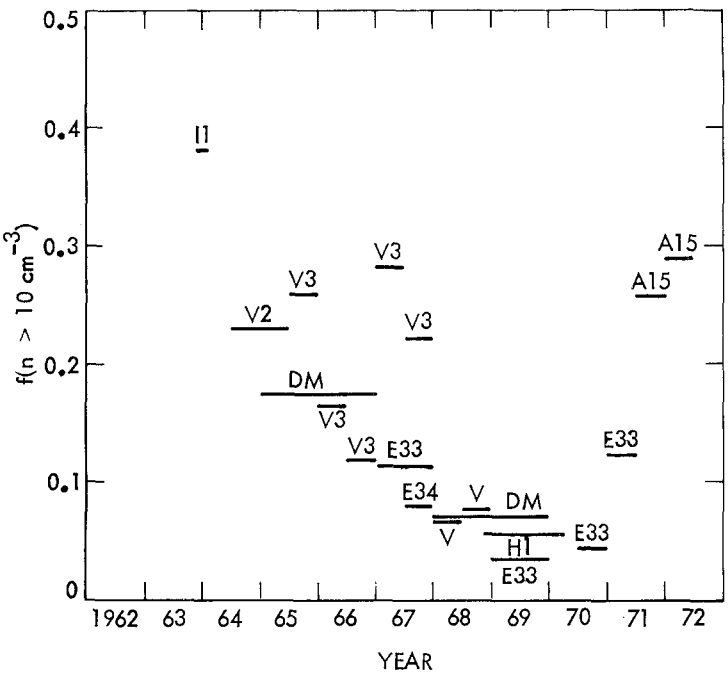

Fig. 26. The fraction of the time that the proton density in the solar wind was observed to be greater than 10 cm^{-3}. The coding is the same as in Figure 23 (see text).

(1970). Figure 27, from Ogilvie and Hirshberg (1974), shows the most recent and thorough analysis of this correlation. The bottom panel shows solar-rotation averages (dots or +) of n_α/n_p, which appear to correlate well with solar activity when averaged over six months or a year (bars) to remove the effect of latitude variations. Unfortunately, the correlation may be somewhat exaggerated by the fact that the data from Explorer 34 and Heos 1 are perhaps overestimated due to relatively high instrument sensitivity thresholds, while spectra for which α-particle data cannot be computed (which can happen for a variety of reasons, one of which is too low an α-flux) are omitted from the OGO-5 averages. Besides the sunspot number, the top of Figure 27

TABLE V

Coefficients in the temperature-velocity relation.
(From Burlaga and Ogilvie, 1973)

$\sqrt{T(10^3\ \mathrm{K})} = a\ V(\mathrm{km\ s^{-1}}) + b$

Probe	Date	a	b
E43	3/18/71–4/8/71	0.033±0.001	−4.8±0.4
E34	6/67–12/67	0.036±0.004	−5.6±1.6
P6	12/18/65–5/4/66	0.032±0.001	−3.3±0.4

shows the best-fit slope of the relation between n_α/n_p and velocity; this correlation with solar activity is apparently very strong, with an enriched helium concentration for a given velocity at times of high solar activity.

4.5. Magnetic field

From bottom to top, Figure 28 shows the time variation of the mean value of the magnitude of the interplanetary magnetic field, the most-probable or modal value of

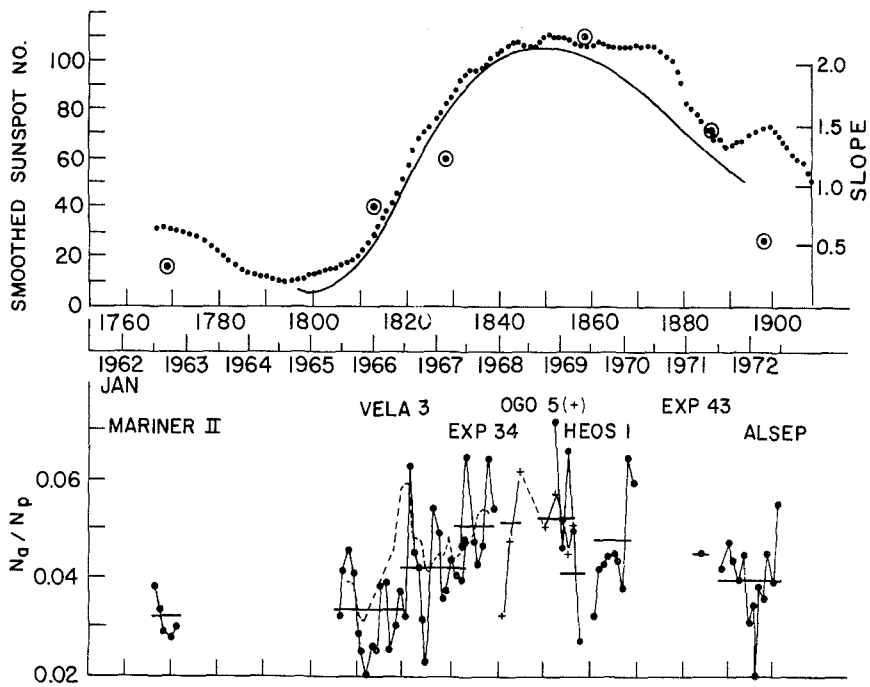

Fig. 27. (Bottom) Solar rotation averages of the ratio of helium to hydrogen densities in the solar wind. The bars represent longer-term averages. (Top) Sunspot number and the slopes (circled dots) of the linear fit between n_α/n_p and velocity (Ogilvie and Hirshberg, 1974).

its magnitude, and the fraction of the time that B is greater than 10 γ. The heavy bars represent yearly values given by Schatten (1971). The shorter bars are other measurements available in the literature. The notation and data sources are: I1 is Imp 1 (Ness, 1968); I2 is Imp 2 (Fairfield and Ness, 1967); and E33 is Explorer 33 (Hirshberg, 1969 and 1973). The values plotted are slightly dependent on the methods of calculation; i.e., on whether one draws histograms from individual measurements or from hourly, or other, averages, and on whether one computes the magnitude of the field before or after finding the time averages of the individual components. Solar-cycle modulation of the field strength is seen in each of the three frames of Figure 28, and depends on the choice of parameter only in detail. This solar-cycle dependence of

magnetic-field strength was previously pointed out by Hirshberg (1969, 1973) and Schatten (1971).

Some solar-cycle variation of the direction of the interplanetary magnetic field has already been discussed in connection with the latitude dependencies shown in Figures 20 and 21. The solar-cycle evolution of the magnetic sector structure is shown in Figure 29 from Wilcox and Colburn (1972). According to geomagnetic records going back

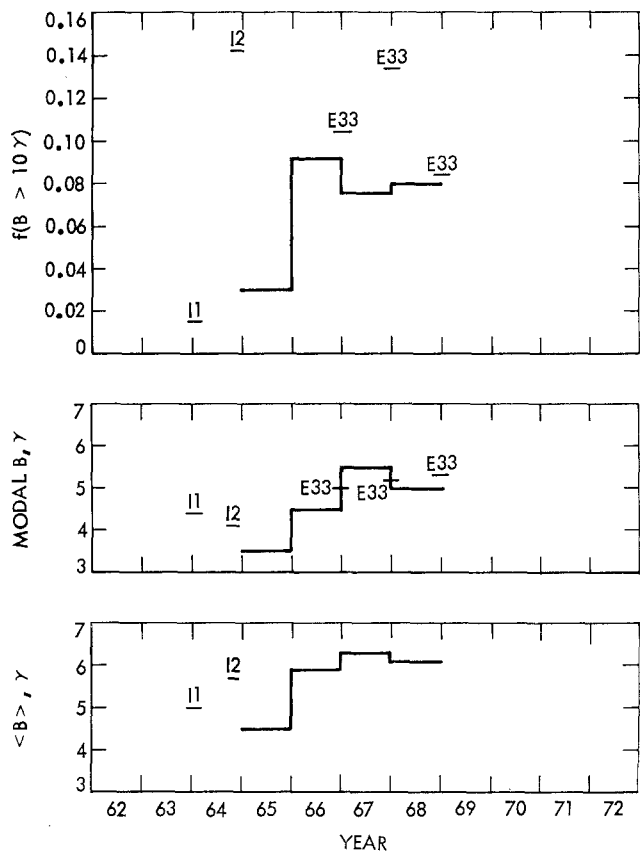

Fig. 28. Time variations of (bottom) the average magnitude of the interplanetary magnetic field, (middle) the most-probable field magnitude, and (top) the fraction of the time the field magnitude is greater than 10 γ. See text for notation and data sources.

to 1926, some of the patterns seen in Figure 29 also existed during other solar cycles. Svalgaard (1972) reports that the rotation period of the magnetic sector structure varies from about 28.5 days in the beginning of a solar cycle (which shows up as a 1–1/2 day advance of the sector boundaries per line of Figure 29, as in late 1965) to 27.0 days at the end (vertical sector boundaries in Figure 29). Svalgaard also finds a high probability of observing four sectors at the beginning of a solar cycle and a frequent disappearance of the sector structure near sunspot minimum.

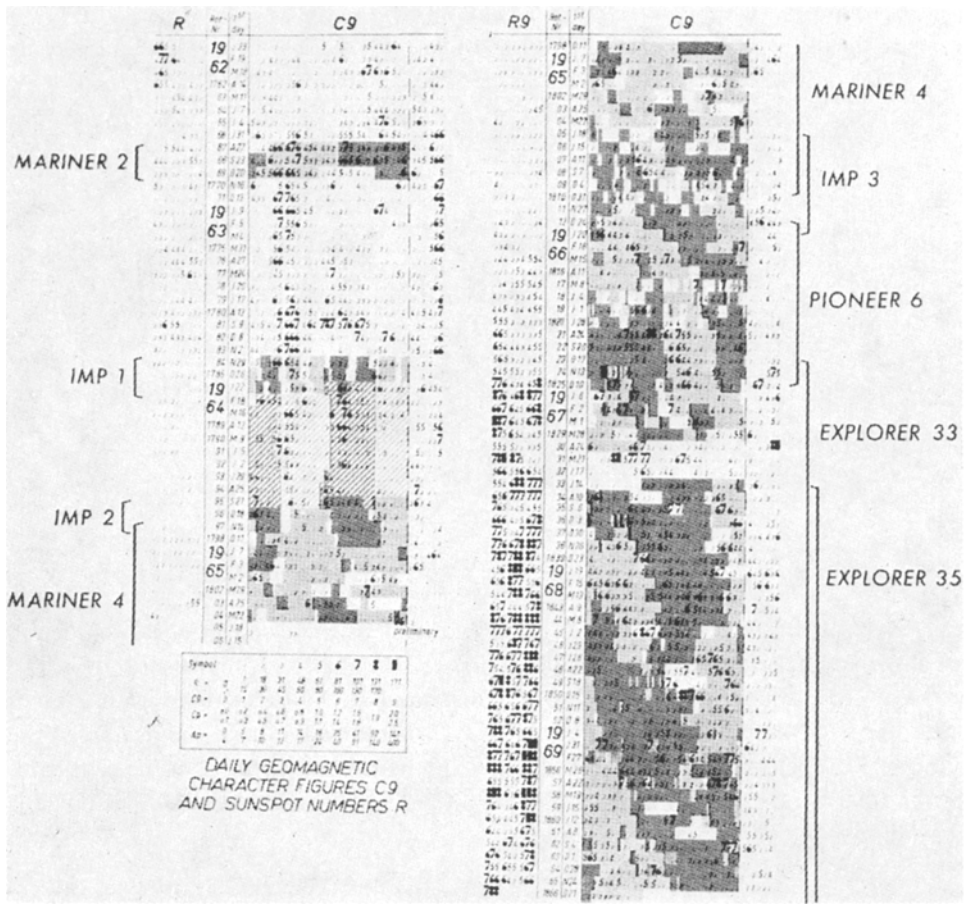

Fig. 29. Observed sector structure of the interplanetary magnetic field. Light (dark) shading indicates a field away from (toward) the Sun. Diagonal bars represent interpolated values (Wilcox and Colburn, 1972).

5. Summary and Conclusions

Table VI provides a very simplified summary of the radial (R), latitude (θ), and solar-cycle (T) variations of the principal properties of the solar wind. A 'yes' in Table VI means a correlation has been observed. Some of these correlations are complex. For example, there is a 'yes' in the R column for V_R because the distribution of V_R is a function of R although the average is not. A question mark in Table VI means that some relevant data have been obtained and analyzed, but that the functional relation is not clear. The fact that there are no 'no' entries means that no parameter has been shown to remain unchanged with distance, latitude, or phase of the solar cycle. The many blank spaces correspond to lacks of observations and/or analyses. There are also many important properties of the solar wind which are not included in Table VI.

TABLE VI

Summary of the observations of the radial (R), latitude (θ), and long-term (T) variations of the properties of the solar wind. A blank means no observations reported

Parameter	R	θ	T	Parameter	R	θ	T
V_R	Yes	Yes	?	T_e	Yes		
V_ϕ	Yes	Yes		N_α/N_p		Yes	Yes
V_θ	Yes			B	Yes		Yes
$\sigma^2(V)$	Yes			B_r	Yes		
N	Yes	Yes	Yes	B_ϕ	Yes		
$\sigma^2(N)$	Yes			B_θ	Yes	Yes	
T_p	Yes		?	$\sigma^2(B)$	Yes		
$T_\parallel/T_\perp$				Polarity		Yes	Yes

For example, measurements of the radial gradient of the electron heat conduction would have important applications to theories of the solar-wind expansion. It is also necessary to cover a much greater range of distances and latitudes. The termination of the solar wind may occur at some tens of AU or more. We have only sampled the fringes of the belt of maximum solar activity and have very little idea of the properties of the solar wind at even higher latitudes up to any polar coronal hole. It is obvious that a lot of work remains to be done.

Acknowledgements

I would like to thank E. J. Smith, J. H. Wolfe, K. W. Ogilvie, P. J. Coleman, Jr., and R. L. Rosenberg for their generous support in supplying data and/or figures for this review prior to publication elsewhere. Helpful information and comments were given by E. J. Smith, F. L. Scarf, D. S. Intriligator, and B. E. Goldstein. This paper presents results of one phase of research carried out at the Jet Propulsion Laboratory, California Institute of Technology, under Contract No. NAS7-100, sponsored by the National Aeronautics and Space Administration.

References

Bame, S. J., Felthauser, H. E., Hundhausen, A. J., Strong, I. B., Asbridge, J. R., Gilbert, H. E., Smith, D. M., and Sydoriak, S. J.: 1970, *A Compilation of Vela 3 Solar Wind Observations, 1965 to 1967*, Los Alamos Scientific Laboratory, LA-4536, Vol. 1.

Bollea, D., Formisano, V., Hedgecock, P. C., Moreno, G., and Palmiotto, F.: 1972, in C. P. Sonett, P. J. Coleman, Jr., and J. M. Wilcox (eds.), *Solar Wind*, NASA SP-308, p. 588.

Brandt, J. C. and Heise, J.: 1970, *Astrophys. J.* **159**, 1057.

Burlaga, L. F.: 1971, *J. Geophys. Res.* **76**, 4360.
Burlaga, L. F. and Ness, N. F.: 1968, *Can. J. Phys.* **46**, 5962.
Burlaga, L. F. and Ogilvie, K. W.: 1970, *Astrophys. J.* **159**, 659.
Burlaga, L. F. and Ogilvie, K. W.: 1973, *J. Geophys. Res.* **78**, 2028.
Coleman, P. J., Jr. and Rosenberg, R. L.: 1971, *J. Geophys. Res.* **76**, 2917.
Coleman, P. J., Jr., Smith, E. J., Davis, L., Jr., and Jones, D. E.: 1969, *J. Geophys. Res.* **74**, 2826.
Coles, W. A. and Maagoe, S.: 1972, *J. Geophys. Res.* **77**, 5622.
Coles, W. A., Rickett, B. J., and Rumsey, V. H.: 1974, in C. T. Russell, (ed.), *Solar Wind Three*, Univ. California, Los Angeles, p. 351.
Collard, H. R., Mihalov, J. D., and Wolfe, J. H.: 1973, (abstract) *EOS, Trans. Am. Geophys. Union* **54**, 1197.
Coon, J. H.: 1968, in B. M. McCormac (ed.), *Earth's Particles and Fields*, Reinhold, New York.
Dessler, A. J.: 1967, *Rev. Geophys.* **5**, 1.
Diodato, L. and Moreno, G.: 1974, *Astrophys. Space Sci.* **28**, L7.
Diodato, L., Moreno, G., Signorini, C., and Ogilvie, K. W.: 1974, *J. Geophys. Res.* **79**, 5095.
Dryer, M.: 1974, *Space Sci. Rev.* **15**, 403.
Dryer, M., Smith, Z. K., Unti, T., Mihalov, J. D., Smith, B. F., Wolfe, J. H., Colburn, D. S., and Sonett, C. P.: 1974, 'Pioneer 9 and OGO-5 Observations of an Interplanetary Multiple Shock Ensemble on 2 February 1969', preprint.
Egidi, A. and Signorini, C.: 1974, *Solar Phys.* **34**, 247.
Fairfield, D. H. and Ness N. F.: 1967, *J. Geophys. Res.* **72**, 2379.
Gosling, J. T., Hansen, R. T., and Bame, S. J.: 1971, *J. Geophys. Res.* **76**, 1811.
Gosling, J. T, Pizzo, V., Neugebauer, M., and Snyder, C. W.: 1972, *J. Geophys. Res.* **77**, 2744.
Gringauz, K. I., Bezrukikh, V. V., Volkov, G. I., Breus, T. K., Musatov, I. S., Havkin, L. P., and Sloutchenkov, G. F.: 1973, *J. Geophys. Res.* **78**, 5897.
Hirshberg, J.: 1969, *J. Geophys. Res.* **74**, 5814.
Hirshberg, J.: 1973, *Astrophys. Space Sci.* **20**, 473.
Hirshberg, J., Asbridge, J. R., and Bame, S. J.: 1972, *J. Geophys. Res.* **77**, 3583.
Hundhausen, A. J., Bame, S. J., Asbridge, J. R., and Sydoriak, S. J.: 1970, *J. Geophys. Res.* **75**, 4643.
Hundhausen, A. J., Bame, S. J., and Montgomery, M. D.: 1971, *J. Geophys. Res.* **76**, 5145.
Intriligator, D. S.: 1974a, *Astrophys. J.* **188**, L23.
Intriligator, D. S.: 1974b, in C. T. Russell (ed.), *Solar Wind Three*, Univ. Calif., Los Angeles, p. 294.
Intriligator, D. S.: 1974c, 'Initial Results on the Scale Size of Plasma Turbulence in the Asteroid Belt', preprint.
Intriligator, D. S. and Neugebauer, M.: 1974, 'A Search for Solar-Wind Velocity Changes between 0.75 AU and 1 AU', preprint.
Lazarus, A. J.: 1970, (abstract), *EOS, Trans. Am. Geophys. Union* **51**, 413.
Lazarus, A. J. and Goldstein, B. E.: 1971, *Astrophys. J.* **168**, 571.
Lazarus, A. J., Heinemann, M. A., McKinnis, R. W., and Bridge, H. S.: 1973, 'Solar Wind Data from the MIT Plasma Experiments on Pioneer 6 and Pioneer 7', National Space Science Data Center NSSDC 73-08.
Lazarus, A. J., Ogilvie, K. W., and Burlaga, L. F.: 1970, *Solar Phys.* **13**, 232.
Mariani, F., Bavassano, B., Villante, U., and Ness, N. F.: 1973, *J. Geophys. Res.* **78**, 8011.
Mihalov, J. D., Wolfe, J. H., and Smith, E. J.: 1973, (abstract) *EOS, Trans. Am. Geophys. Union* **54**, 1198.
Montgomery, M. D.: 1972, in C. P. Sonett, P. J. Coleman, Jr., and J. M. Wilcox (eds.), *Solar Wind*, NASA SP-308, p. 208.
Moreno, G. and Palmiotto, F.: 1973, *Solar Phys.* **30**, 207.
Ness, N. F.: 1968, *Ann. Rev. Astron. Astrophys.* **6**, 79.
Neugebauer, M. and Snyder, C. W.: 1966, *J. Geophys. Res.* **71**, 4469.
Obayashi, T.: 1968, 'Solar Terrestrial Activity Chart – B', Inter-Union Commission on Solar-Terrestrial Physics.
Ogilvie, K. W.: 1972, *J. Geophys. Res.* **77**, 4227.
Ogilvie, K. W. and Hirshberg, J.: 1974, *J. Geophys. Res.* **79**, 4595.
Olbert, S.: 1968, R. L. Carovillano (ed.), *Physics of the Magnetosphere*, D. Reidel, Dordrecht-Holland, p. 641.
Pinter, S.: 1974, *Solar Phys.* **28**, 477.

Parker, E. N.: 1963, *Interplanetary Dynamical Processes*, Interscience, New York.
Parker, E. N.: 1965, *Space Sci. Rev.* **4**, 666.
Rhodes, E. J., Jr. and Smith, E. J.: 1973, (abstract), *EOS, Trans. Am. Geophys. Union.* **54**, 448.
Rhodes, E. J., Jr. and Smith, E. J.: 1974, *Trans. Am. Geophys. Union* **55**, 409.
Robbins, D. E., Hundhausen, A. J., and Bame, S. J.: 1970, *J. Geophys. Res.* **75**, 1178.
Rosenberg, R. L. and Coleman, P. J., Jr.: 1969, *J. Geophys. Res.* **74**, 5611.
Rosenberg, R. L. and Coleman, P. J., Jr.: 1973, *Inst. Geophys. Planetary Phys.* Publ. No. 1196-26.
Rosenberg, R. L. and Coleman, P. J., Jr.: 1974, 'Radial Dependence of Interplanetary Magnetic Field Power Spectra', in preparation.
Rosenberg, R. L., Coleman, P. J., Jr., and Colburn, D. S.: 1971, *J. Geophys. Res.* **76**, 6661.
Rosenberg, R. L., Coleman, P. J., Jr., and Ness, N. F.: 1973, *J. Geophys. Res.* **78**, 51.
Scarf, F. L. and Wolfe, J. H.: 1974, *J. Geophys. Res.* **79**, 4179.
Scarf, F. L., Green, I. M., and Burgess, J. S.: 1973, *Astrophys. Space Sci.* **20**, 499.
Schatten, K. H.: 1971, *Rev. Geophys. Space Sci.* **9**, 773.
Scudder, J. D., Lind, D. L., and Ogilvie, K. W.: 1973, *J. Geophys. Res.* **78**, 6535.
Smith, E. J.: 1974, in C. T. Russell (ed.), *Solar Wind Three*, Univ. Calif. Los Angeles, p. 257.
Smith, E. J. and Rhodes, E. J., Jr.: 1974, in C. T. Russell (ed.), *Solar Wind Three*, Univ. Calif., Los Angeles, p. 329.
Strong, I. B., Asbridge, J. R., Bame, S. J., and Hundhausen, A. J.: 1967, in J. L. Weinberg (ed.), *The Zodiacal Light and the Interplanetary Medium*, NASA, Washington, DC, p. 365.
Svalgaard, L.: 1972, *J. Geophys. Res.* **77**, 4027.
Wilcox, J. M.: 1970, *J. Geophys. Res.* **75**, 2587.
Wilcox, J. M. and Colburn, D. S.: 1972, *J. Geophys. Res.* **77**, 751.
Wilcox, J. and Scherrer, P.: 1972, *J. Geophys. Res.* **77**, 5385.